IEEE Photonics Journal
An IEEE Photonics Society Publication

Open Access

A Planarized Thermophotovoltaic Emitter With Idealized Selective Emission

Volume 8, Number 4, August 2016

Sze Ming Fu
Yan Kai Zhong
Ming Hsiang Tu
Bo Ruei Chen
Albert Lin

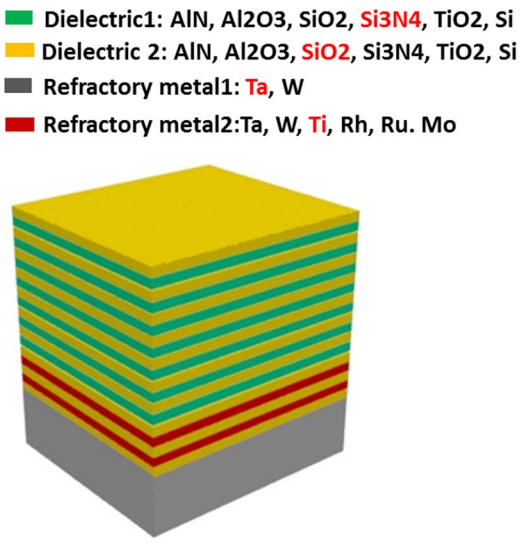

DOI: 10.1109/JPHOT.2016.2594704
1943-0655

A Planarized Thermophotovoltaic Emitter With Idealized Selective Emission

Sze Ming Fu, Yan Kai Zhong, Ming Hsiang Tu, Bo Ruei Chen, and Albert Lin

Department of Electronics Engineering, National Chiao Tung University, Hsinchu 30010, Taiwan

DOI: 10.1109/JPHOT.2016.2594704

Manuscript received June 3, 2016; revised July 20, 2016; accepted July 22, 2016. Date of publication July 27, 2016; date of current version August 9, 2016. This work was supported by the Ministry of Science and Technology of Taiwan under Grant 103WFA0650933. Corresponding author: A. Lin (e-mail: hdtd5746@gmail.com).

Abstract: Compared with conventional solar cells, thermophotovoltaics (TPV) can be more efficient and, thus, exceeds the detailed balance efficiency limit. In particular, the emitter of TPV is a critical design since it determines whether the thermalization loss can be reduced and whether the sub-band-gap radiation can be suppressed, as far as the photovoltaic (PV) process is concerned. In this paper, we propose a selective planar emitter composed of alternating ultrathin metal and dielectric layers. An aperiodic dielectric stacking is designed to tailor the emission spectrum by shaping the emission peak and by adjusting the emission wavelength. We show that the peak emission wavelength $(\lambda_{\text{emission}})$ is adjustable from $\lambda = 1500$ nm to $\lambda = 2500$ nm. Furthermore, the long-wavelength cutoff is very sharp for our proposed emitter structure, and the absorption is suppressed to 0.1 beyond the cutoff. The preliminary experiment is also conducted to fulfill the concept of a fully planar ultrathin refractory metal emitter design, and the result is similar to the calculated ones. We believe that the planar thermal emitter based on ultrathin metals and aperiodic dielectric stacking is very promising for future thermal emission applications since it requires no lithography and etching, provides strong peak emission power, and possesses wide wavelength scalability.

Index Terms: Photovoltaics (PV), optical properties of photonic materials, metamaterial, thin film coatings.

1. Introduction

The thermophotovoltaics (TPV) has been proposed to exceed the efficiency limit of conventional photovoltaics (PV) [1]–[10]. A TPV system is mainly composed of an emitter-absorber stack and a photodiode. The absorber is in charge of sunlight collection where metallic absorption enables a true broadband solar energy harvesting in many cases. The absorber converts the solar energy into heat rather than electron-hole pairs, as is the case in conventional PV systems. The heated absorber-emitter then radiates like a blackbody, and the photodiode beneath absorbs the emitted photons and generates electricity. The most notable improvement of TPV over the conventional PV is that TPV can utilize photons with energy below the semiconductor bandgap and minimize the thermalization loss for the photons with energy much greater than the bandgap [11]–[15]. This improvement comes from the fact that TPV converts the solar photons into thermal energy and then emits a narrow band infrared radiation toward the p-n diode underneath. As a result, how to absorb and emit the solar radiation appropriately is a key factor for an

efficient TPV system. For the spectrum of an ideal emitter, there must be a cut-off in long wavelength regime because these photons are transparent to the photodiode, and the emission peak should be just slightly above the diode bandgap and of narrow-band nature, in order to minimize the thermalization loss associated with the high energy photons.

A closely related field of TPV emitter design is the metamaterial perfect absorbers (MPA) [16]–[22]. The more challenging aspect of TPV emitter design is that the selection of the metal is limited to the refractory ones, and the selective, instead of broadband unity emittance (i.e., absorbance), is necessary. In literature, there have been various effort in thermophotovoltaic (TPV) emitters [1], [2], [4]–[6], [23], [24]. Among these efforts, Rinnerbauer *et al.* propose the use of Ta-based photonic crystals (PhC) [2], [4], [23], which is the highest performance and highest temperature design to date based on our literature review. The slight drawback of this structure is the deep trench etching into Ta substrate and the potential surface diffusion of metal at elevated temperature. Shvet *et al.* propose the use of tungsten (W) based metal-dielectric nanostructures with the capability of rolling around [1]. Other decent structures include the SiO_2-Si planar stacking, and its fully planarized nature is promising [5]. The theoretical work by Bermel *et al.* is also interesting, which calculates the spectral responses of a double side filtering structure with erbium-doped aluminum garnet (ErAG) as thermal emission materials [25].

In this work, we propose a fully planar TPV emitter structure without the need for any lithography and etching, using ultrathin refractory metal. Such a planar structure not only promotes low-cost and large-area emitters but possesses decent performance, compared to many nanostructured designs, as well. Additionally, the selection of the dielectric multi-layer materials is commented in the experimental section since the MWIR absorption of many real dielectrics can be an issue in practice [26]. Compared to Ta-based PhC [2], [4], [23], our proposal eliminates the need of deep trench etching and potential metal surface diffusion at high temperature. Compared to the double side filtering structure using erbium-doped aluminum garnet (ErAG) wafer [25], our proposal has reduced thickness and only requires a single side dielectric filter with a reduced pair number. The emitter thickness in [25] is > 100 μm, while the emitter thickness in this work is < 5 μm. Compared to the tungsten (W) based metal-dielectric nanostructures with the capability of rolling around [1], our proposal eliminates the need of lithography and etching.

2. The Proposed Planar Ultrathin Metal Emitter Design

The calculation method is based on rigorously coupled wave analysis (RCWA), and the simulation software is RSoft DiffractMOD [27]. The material parameters are from RSoft database. Because the emission spectrum is strongly related to the layer thicknesses of the thin metal and dielectrics, the genetic algorithm (GA) is selected to locate all of the geometry parameters including the layer thickness and the number of the deposited layer necessary for an ideal response [28]–[32]. Since the geometry is planar, no lithography and etching is needed, which is a promising feature in this design. Fig. 1 shows the proposed structure in this work.

In Fig. 1(a) and (b), we show the set-up of a standard TPV system and the ideal TPV emitter and absorber spectral characteristics. The filter is optional and mostly absent in modern designs, and therefore a selective emitter is necessary. A narrow to moderate emission bandwidth is desired as far as the TPV emitter is concerned. In Fig. 1(c) and (d), we show the schematic drawing of the proposed emitter structure with dimensions labeled. The emitter is constructed on the bottom metallic layer. In this study, we choose tantalum (Ta) as the bottom plate metal1 material, and tungsten (W) is also usable. Ta has a high extinction coefficient (k) than W, and can be advantageous in long wavelength high reflection, i.e., low absorption. Nevertheless, W has a slightly higher melting point. Depending on thermal emission applications, this metal1 can also be other refractory metals, but for TPV, Ta or W is more suitable. Afterward, metal2 and dielelctric2 alternating layers are deposited on metal1, and the thicknesses of metal2/dielectric2 are optimized by GA. Similarly, metal2 can also be any refractory metals, such as Ta, W, Rh, Ru, Ti, etc., depending on specific applications. Here, we choose titanium (Ti) as metal2. Ti has slowly increased extinction (k) with wavelength, and this is beneficial for narrow-bandwidth to

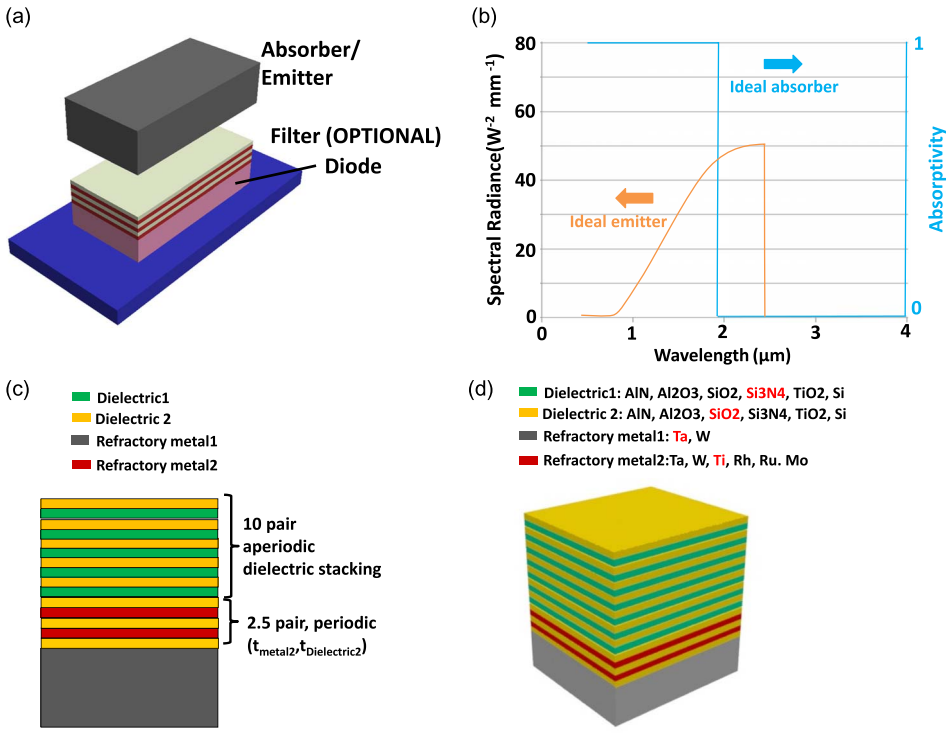

Fig. 1. (a) Schematic of the TPV system. (b) Ideal emitter/absorber spectral responses. (c) Proposed emitter structure in 2-D drawing. The layer/material annotation and the thickness symbols are shown. (d) Three-dimensional view of the proposed thermal emitter and the potential material combinations. The selection of the metal and the dielectric materials is of wide flexibility in our proposed planar configuration. The list of the candidate materials is included. The selected materials in this work are labeled in red.

moderate-bandwidth emission using a relatively small number of periodic stacking with ultrathin-metal and dielectric. Using Ta or W can benefit a really high-temperature operation, but due to their higher k values, more periodic stacking layers are necessary to achieve a narrow-band emission peak. A narrow to moderate emission bandwidth is beneficial for TPV because this reduces the thermalization of high energy photons and at the same time maintains noticeable IR emission toward the photodiode. After periodic metal2-dielectric2 stacking, an aperiodic dielectric stacking, consisting of dielectric1-dielectric2 alternating layers, is constructed on top of the emitter. In this work, we choose Si_3N_4-SiO_2. The layer thickness of the aperiodic stacking can affect the spectral response of the emitter. Namely, we can shift the emission peak or shape the spectral response by adjusting the geometry. In this work, the emission peak is set between $\lambda_{\text{emission}} = 1500$ nm to $\lambda_{\text{emission}} = 2500$ nm.

3. Simulation Result

Fig. 2 shows the spectral emittance for the proposed structure. The emission wavelength is scalable by adjusting the aperiodic stacking layer thickness and the dielectric spacer thickness $(t_{\text{Dielectric2}})$ between the ultra-thin metals (t_{metal2}). The wavelength scalability is desired for many photonic applications. The high emittance at the emission wavelength $(\lambda_{\text{emission}})$ is due to the proper design of the aperiodic stacking where the photon confinement is enhanced at $\lambda_{\text{emission}}$. The long-wavelength suppression in emittance is due to the gradually increased extinction coefficients (k) of Ta with wavelength, which leads to excessive reflection. In addition, due to the large dimension ratio between the photon wavelength and t_{metal2}, the ultra-thin metallic film is invisible at the long wavelength regime. As a result, the bulk property of Ta substrate is predominant, and the high reflectance directly gives low emittance since photons cannot penetrate into the

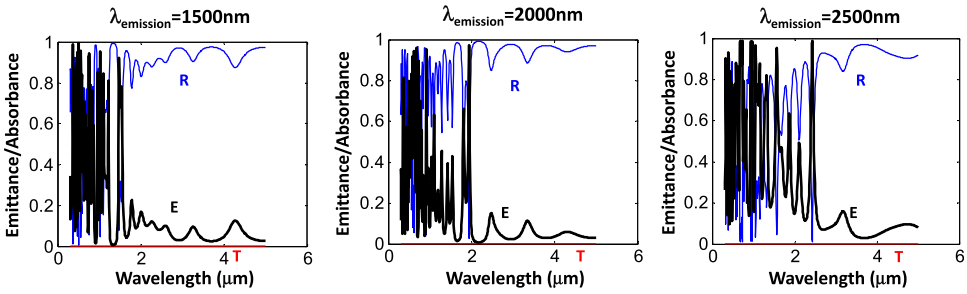

Fig. 2. Reflectance (R), transmittance (T), and absorbance/emittance (A/E) versus wavelength. The shift of peak emission wavelength, i.e., $\lambda_{emission} = 1500$ nm to $\lambda_{emission} = 2500$ nm, is achieved with different geometries of ultrathin metals and the aperiodic dielectric layers. The individual layer thickness can be found in Table 1.

TABLE 1

Layer thicknesses of the selective thermal emitters. The metal2–dielectric2 stacking is periodic, and the dieelctric1–dielectric2 stacking is aperiodic. The unit is in micrometers (μm)[a]

$\lambda_{emission}$	t_{metal2}	$t_{Dielectric2}$	L1	L2	L3	L4
1500nm	0.005	0.010	0.346	0.377	0.157	0.149
2000nm	0.002	0.010	0.029	0.149	0.323	0.230
2500nm	0.005	0.031	0.488	0.029	0.083	0.411
$\lambda_{emission}$	L5	L6	L7	L8	L9	L10
1500nm	0.257	0.211	0.257	0.106	0.380	0.133
2000nm	0.072	0.010	0.265	0.296	0.187	0.315
2500nm	0.400	0.330	0.087	0.153	0.118	0.299
$\lambda_{emission}$	L11	L12	L13	L14	L15	L16
1500nm	0.214	0.199	0.099	0.257	0.118	0.141
2000nm	0.230	0.276	0.118	0.022	0.388	0.299
2500nm	0.230	0.465	0.496	0.434	0.072	0.361
$\lambda_{emission}$	L17	L18	L19	L20	-	-
1500nm	0.195	0.330	0.153	0.118	-	-
2000nm	0.380	0.218	0.369	0.122	-	-
2500nm	0.257	0.014	0.400	0.010	-	-

[a] The order of the list is from the bottom layer to the topmost layer. L1 is SiO_2, L2 is Si_3N_4, L3 is SiO_2, and etc.

absorbing medium. The long wavelength emittance suppression is very critical for TPV. This is because the semiconductor diode beneath the TPV emitter has a fixed bandgap energy (E_G). Thus, long wavelength emission cannot be absorbed by the p-n junction diode. In this study, we use a genetic algorithm to adjust the layer thickness in order to boost the emittance at $\lambda_{emission}$ and to suppress the emittance at long wavelength. For an ideal TPV emitter, the very-short-wavelength emittance should also be suppressed to reduce the thermalization loss. We have to point out that GA can certainly achieve this, and in order to reach this goal, a more elaborate aperiodic dielectric stacking may be needed. Fortunately, a simple 10-pair (10X) dielectric stacking in this work still leads to a satisfactory result. We see that the emittance at the short wavelength side near the $\lambda_{emission}$ is suppressed. For the very short wavelength regime, the emitted power will decay by itself due to the Plank's law for blackbody radiation, and thus the emittance values at the very-short-wavelength regime are less critical.

The angular response is shown in Fig. 3. We can see that as the incidence angles deviate from the normal direction, the high emittance value is still maintained. This omnidirectionality characteristic is observed in other TPV emitter configurations in the literature [1], [2], [4]–[6], [23], [24]. Depending on the applications, the omnidirectionality can be preferred or not preferred. For many thermal emission devices, the emitted power needs to be of wide-angle nature for a maximized efficiency. As far as the TPV is concerned, since, in most of the current TPV systems, the emitter and the solar panel arrays are very closely spaced [5], and III-V high-performance solar cells are employed, the angular emission characteristic is less important. Both the normally

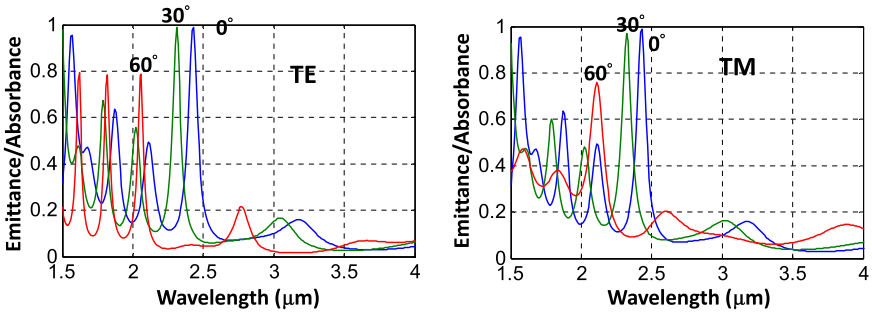

Fig. 3. Angular spectral absorbance (A)/emittance (E) of the selective emitter, targeting at $\lambda = 2.5$ μm for (a) TE and (b) TM polarizations. The individual layer thickness can be found in Table 1.

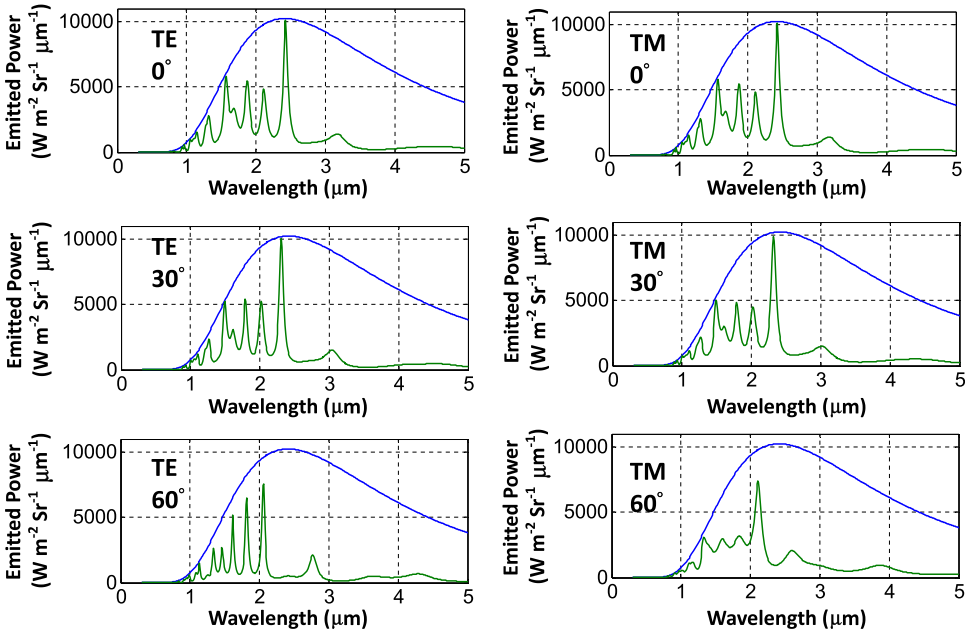

Fig. 4. Emission spectrums for different incident angles (0°, 30°, and 60°) for an ideal blackbody (blue) and the proposed selective emitters (green). The individual layer thickness can be found in Table 1.

emitted power and the obliquely emitted power can be collected by the solar cells directly under the TPV emitter. If lower cost perovskite, silicon, or silicon germanium thin film solar cells are used, and the solar cell panel area is much greater than the emitter itself, the omnidirectional emission becomes desirable. Fig. 4 plots the emitted power versus wavelength at various emission angles, for the case of $\lambda_{\text{emission}} = 2500$ nm. The spectral emitted energy of an ideal black body in unit of power per unit solid angle per unit area and per unit wavelength (W m^{-2} Sr^{-1} mm^{-2}) can be written down using Plank's formula

$$B_\lambda(\lambda, T) = \frac{2hc^2}{\lambda^5} \frac{1}{\exp\left(\frac{hc}{\lambda k_B T_{\text{TPV}}}\right) - 1} \tag{1}$$

where h is Planck's constant, k_B is Boltzmann constant, λ is the free space wavelength, c is the speed of the light, and T_{TPV} is the temperature of the TPV emitter-absorber stack. The total emitted power can be expressed using Stefan-Boltzmann law:

$$P_{\text{emit}} = A\sigma\varepsilon T_{\text{TPV}}^4 \tag{2}$$

where A is the surface area of the black body, σ is Stefan Boltzmann constant, and ε is the emittance with values between 0 and 1, which is the values plotted in Fig. 3. For an ideal black body (BB), ε equals unity for a broad spectral range. The emitter design here uses the convention that the emittance peak coincides with the black body radiation peak in the wavelength axis. To achieve this, the temperature of the emitter should be adjusted accordingly. Therefore, 1200 K is chosen for the selective thermal emitter with the emittance peak at $\lambda_{\text{emission}} = 2500$ nm.

4. Experiment

In order to realize the proposal, the initial experiment is conducted. First, 200 nm Ta is deposited as a bottom layer on a silicon wafer using ULVAC ENTRON W200 sputterer. Afterward, two pairs of SiO_2 and Ti are deposited alternately by an AST PEVA 600I electron-gun (e-gun) evaporator. The pressure in depositing Ti and SiO_2 are 3×10^{-6} torr and 5×10^{-6} torr, and the thickness of Ti and SiO_2 are 5 nm and 10 nm, respectively. Finally, ten pairs of SiO_2 and Si_3N_4 are deposited alternately by plasma-enhanced chemical vapor deposition (PECVD). Silane (SiH_4) and nitrous oxide (N_2O) are the precursors in depositing SiO_2 layers. The temperature and pressure is 300 °C and 100 mtorr. Si_3N_4 layers are deposited with SiH_4 and ammonia (NH_3) at 300 °C in 100 mtorr. The thickness of SiO_2 and Si_3N_4 are different in each layer since we have an aperiodic dielectric1-dielectric2 stacking.

The reflectance (R) and transmittance (T) of the selective thermal emitter are measured by Bruker IFS66V/S Fourier transform infrared spectroscopy (FTIR) system to measure the reflectance and transmittance from $\lambda = 1260$ nm to $\lambda = 10\,000$ nm. Emittance (E), or equivalently absorbance (A), can be calculated by 1-reflectance (R)-transmittance (T). Fig. 5(a) shows the experimental results of the reflectance, transmittance, and emittance for our selective planar emitter with emission wavelength at $\lambda_{\text{emission}} = 1500$ nm. The absorbance at $\lambda = 1500$ nm is over 95%, and therefore, the proposed emitter exhibits a decent emission. In the physical process of photon propagation, the gradually increased extinction coefficients of tantalum (Ta) lead to an absorption/emission cut-off in the long wavelength regime. This is because the increased k can lead to large field and power reflection coefficients. The measured result in Fig. 5(a) is consistent with the calculation result in Fig. 2 where a peak emission exists at $\lambda_{\text{emission}} = 1500$ nm, and the emittance decays dramatically at $\lambda > \lambda_{\text{emission}}$. The slight discrepancy in Fig. 5(a) is that the suppressed emittance from $\lambda = 1700$ nm to $\lambda = 4000$ nm is slightly higher than the calculated result, due to the surface and interface roughness of the deposited layers. The sample roughness effect will be explained later together with atomic force micrograph (AFM) data. Compared with the state-of-the-art Ta PhC design [2], [4], [23], the proposed planar emitter here possesses comparable spectral emittance characteristics. Specifically, the peak emittance values at $\lambda_{\text{emission}}$ in both designs are close to unity. In addition, the long wavelength suppressed emittance in our calculated result is 0.1 in Fig. 2, similar to the calculated results in the Ta PhC [2], [4], [23]. The measured emittance at $\lambda > \lambda_{\text{emission}}$ is 0.3 in our design, slightly higher than the value of 0.2 in the Ta PhC. The reason is that a polished Ta substrate is used in the Ta PhC emitter [2], [4], [23]. Finally, a single narrow-band emission peak at $\lambda = \lambda_{\text{emission}}$ is observed in our proposed planar emitter, while in the Ta PhC emitter, the emittance does not decrease dramatically at $\lambda < \lambda_{\text{emission}}$. In this aspect, our design leads to less thermalization loss since the emitted power decreases more sharply at $\lambda < \lambda_{\text{emission}}$ in our design compared to the Ta PhC.

Fig. 5(b) shows the FTIR measurement until $\lambda = 10\,000$ nm. It is worth to mention that from the FTIR result in Fig. 5(b), the emitter has strong absorption at $\lambda = 4500$ nm and $\lambda = 8000$ nm, corresponding to the Si_3N_4 and SiO_2 absorption band. In fact, the long wavelength absorption is not detrimental since the ideal black body emission spectrum decays rapidly at long wavelength. In Fig. 5(b), we also plot the black body spectrum at 1800 K, and it can be seen that at Si_3N_4 absorption band at $\lambda = 4500$ nm [26], the black body radiation already decays to a much lower value compared to its peak emitted power. Based on Carnot efficiency $\eta = 1 - T_{\text{ambient}}/T_{\text{TPV}}$, the higher the TPV emitter temperature (t_{TPV}) is, the higher the efficiency of the system. The black body of 1800 K is plotted here because $t_{\text{TPV}} = 1800$ K has been shown to be the practical TPV

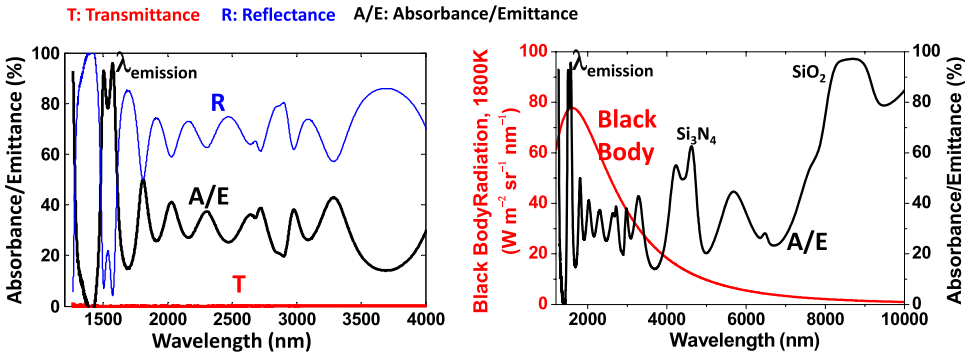

Fig. 5. (a) Measured FTIR spectral responses of the fabricated sample at $\lambda = 1200 - \lambda = 4000$ nm. (b) Measured FTIR spectral responses of the fabricated sample at $\lambda = 1200 - \lambda = 10\,000$ nm and an ideal black body spectrum at 1800 K. The silicon nitride (Si_3N_4) and silicon oxide (SiO_2) absorption bands at long-wavelength regime do not affect the thermal emitter operation if t_{TPV} 1800 K is used. Lower t_{TPV} requires replacement of silicon nitride with other dielectrics. The individual layer thickness can be found in Table 1.

high-temperature operation limit. If the operation temperature of the TPV emitter is lowered, the Si_3N_4 absorption can be a problem since the black body radiation may still have some radiated power around $\lambda = 4.5$ μm. In order to resolve the issue at lower t_{TPV}, we can replace Si_3N_4 with other materials such as TiO_2, Al_2O_3, AlN, or Si [26], [33]. From the refractive indices measurement data at room temperature in the literature [26], [33], Si_3N_4 has gradually increased k from $\lambda = 5$ μm, while SiO_2 and TiO_2 have negligible k until $\lambda = 7$ μm. Si, on the other hand, is transparent until $\lambda = 10$ μm. The advantage of using Si_3N_4 is that it is entirely compatible with standard silicon IC processing. Using TiO_2 or Si has the benefit of less residual absorption at long wavelength while the disadvantage of Si is that it is thermally active material by itself, and the disadvantage of TiO_2 is that it is less common in standard IC processing.

The surface and interface roughness can have an effect on the absorption suppression at $\lambda =$ 1750 nm to $\lambda = 4000$ nm in Fig. 5(a). Ideally, a fully suppressed absorbance, i.e. high reflectance, beyond cut-off is desired, and the simulation result indeed shows an emittance values ~0.1 for our proposed thermal emitter structure. Nevertheless, the surface roughness can lead to more absorption at long wavelength due to the enhanced absorbance by random light scattering. The effect of surface and interface random texture on photon absorption/emission process has been fully investigated in solar cell light trapping literature. It has been known for years that the randomly textured surface is very effective in photon confinement and absorption enhancement [34]–[37]. In addition, the roughness value for metallic textures needed for light trapping is much smaller than dielectric textures. This is due to the much greater scattering and absorption cross sections of the metallic nanostructures, caused by the distinct dielectric functions of metals compared to semiconductors or dielectrics. It has been shown that 10 nm to 20 nm plasmonic nanoparticles can have a large far-field scattering cross-section [38]. In our cases, the ultrathin Ti films are very absorptive, and slight textures on the interface between Ti and SiO_2 can lead to strong near-field absorption/emission enhancement. Atomic force microscope (AFM) is used to confirm the surface roughness (see Fig. 6). Table 2 provides the atomic force microscope (AFM) root-mean-square roughness values, measured by Digital Instrumen AFM-D3100. The root mean square roughness (σ_{RMS}) is 3.13 nm for our finished emitter sample top surface, and the individual material roughness values are also provided. Using e-gun and sputter can be less effective for achieving fully uniform and smooth films. Other deposition methods such metal–organic chemical vapor deposition (MOCVD) and atomic layer deposition (ALD) can be beneficial in this aspect. In fact, a polished Ta substrate has been used in literature, and this can further decrease the long-wavelength residual emittance/absorbance [2], [23].

Finally, it is worth pointing out that in this work, we only use an e-gun evaporator (PECVD) and a sputter to construct the ultrathin metal and the aperiodic dielectric stacking, and therefore,

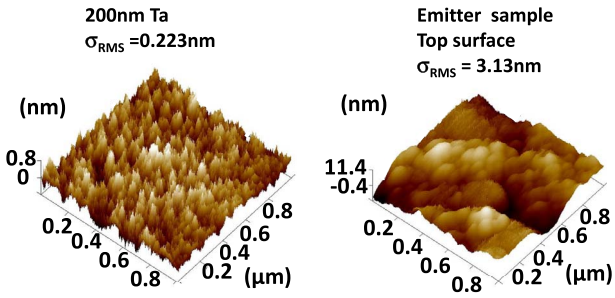

Fig. 6. AFM for (a) 200-nm Ta bottom plate and (b) the finished thermal emitter sample top surface.

TABLE 2

Root-mean-square roughness σ_{RMS} of the AFM micrographs

Layer Description	σ_{RMS} (nm)
Polished Si wafer	0.178
200nm sputtered Ta on polished Si wafer	0.223
5nm sputtered Ta ultrathin film on polished Si wafer	0.170
2nm e-gun Ti on polished Si wafer	0.33
15nm e-gun silicon dioxide on polished Si wafer	0.859
200nm PECVD silicon dioxide on polished Si wafer	1.53
200nm PECVD silicon nitride on polished Si wafer	1.8
The top surface of the finished emitter sample	3.13

the fabrication is free of lithography and etching. This makes the proposed thermal emitter structure fully scalable to large-area devices at relatively low cost.

5. Conclusion

In this work, we propose a planar emitter structure composed of periodic ultrathin-metal-dielectric stacking and aperiodic dielectric stacking. It is shown that the spectral response of this planar emitter structure is close to the ideal one where strong peak emission and suppressed long wavelength emission are all achieved. The purpose of using the aperiodic dielectric layers is to shape the thermal emission spectrum in terms of the shape and the emitted power, especially near the peak emission wavelength. A narrow-band and sharp emission peak is thus formed. Also, the wavelength of emission peak can be shifted by adjusting the layer thickness of the aperiodic dielectric stacking layers, leading to wavelength scalability. The aperiodic stacking is composed of the SiO_2-Si_3N_4 alternating layers, and genetic algorithm (GA) is used to optimize the aperiodic structure. Finally, we also conduct the initial experiment to fulfill the concept of a planar ultrathin-metal thermal emitter. A 200 nm Ta layer is deposited as the bottom plate to suppress the long wavelength absorption, owing to its high extinction coefficient and high reflectance in the long wavelength regime. The measured absorbance/emittance agrees with our theoretical prediction in that the emission peak exists at predicted $\lambda_{emission} = 1500$ nm, and a long wavelength cut-off is observed. The dielectric absorption bands of Si_3N_4 and SiO_2 are observed at the mid-wave infrared (MWIR) regime, and it is shown that the Si_3N_4 absorption band at 4.5 μm does not affect the feasibility of our design at TPV practically-optimal high-temperature operation at 1800 K. The selection of other dielectric materials is suggested based on their extinction coefficients, which can benefit lower temperature TPV system operation. Further experiment effort can be in reducing the surface roughness of the metal and dielectric thin films. We believe the proposed thermal emitter in this paper is competitive in terms of fabrication complexity and spectral emission characteristic.

References

[1] C. Wu *et al.*, "Metamaterial-based integrated plasmonic absorber/emitter for solar thermo-photovoltaic systems," *J. Opt.*, vol. 14, 2012, Art. no. 024005.
[2] V. Rinnerbauer *et al.*, "Metallic photonic crystal absorber-emitter for efficient spectral control in high-temperature solar thermophotovoltaics," *Adv. Energy Mater.*, vol. 4, 2014, Art. no. 1400334.
[3] R. E. Nelson, "A brief history of thermophotovoltaic development," *Semicond. Sci. Technol.*, vol. 18, p. S141, 2003.
[4] Y. Nam *et al.*, "Solar thermophotovoltaic energy conversion systems with two-dimensional tantalum photonic crystal absorbers and emitters," *Sol. Energy Mater. Sol.*, vol. 122, pp. 287–296, 2014.
[5] A. Lenert *et al.*, "A nanophotonic solar thermophotovoltaic device," *Nature Nanotechnol.*, vol. 9, pp. 126–130, 2014.
[6] P. Bermel *et al.*, "Design and global optimization of high-efficiency thermophotovoltaic systems," *Opt. Exp.*, vol. 18, pp. A315–A334, 2010.
[7] P. A. Davies and A. Luque, "Solar thermophotovoltaics: Brief review and a new look," *Sol. Energy Mater. Sol.*, vol. 33, pp. 11–22, 1994.
[8] Z. Zhou, Q. Chen, and P. Bermel, "Prospects for high-performance thermophotovoltaic conversion efficiencies exceeding the Shockley-Queisser limit," *Energy Convers. Manage.*, vol. 97, pp. 63–69, 2015.
[9] C. Ferrari, F. Melino, M. Pinelli, P. R. Spina, and M. Venturini, "Overview and status of thermophotovoltaic systems," *Energy Procedia*, vol. 45, pp. 160–169, 2014.
[10] H. Daneshvar, R. Prinja, and N. P. Kherani, "Thermophotovoltaics: Fundamentals, challenges and prospects," *Appl. Energy*, vol. 159, pp. 560–575, 2015.
[11] A. D. Vos, "Detailed balance limit of the efficiency of tandem solar cells," *J. Phys. D, Appl. Phys.*, vol. 13, pp. 839–846, 1980.
[12] W. Shockley and H. Queisser, "Detailed balance limit of efficiency of p-n junction solar cell," *J. Appl. Phys.*, vol. 32, pp. 510–519, 1961.
[13] A. S. Brown and M. A. Green, "Detailed balance limit for the series constrained two terminal tandem solar cell," *Physica E*, vol. 14, pp. 96–100, 2002.
[14] G. Wei, K.-T. Shiu, N. C. Giebink, and S. R. Forrest, "Thermodynamic limits of quantum photovoltaic cell efficiency," *Appl. Phys. Lett.*, vol. 91, 2007, Art. no. 223507.
[15] G. Wei and S. R. Forrest, "Intermediate-band solar cells employing quantum dots embedded in an energy fence barrier," *Nano Lett.*, vol. 7, pp. 218–222, 2007.
[16] Y. Ra'di, C. R. Simovski, and S. A. Tretyakov, "Thin perfect absorbers for electromagnetic waves: Theory, design, and realizations," *Phys. Rev. Appl.*, vol. 3, 2015, Art. no. 037001.
[17] H. Tao *et al.*, "A dual band terahertz metamaterial absorber," *J. Phys. D, Appl. Phys.*, vol. 43, 2010, Art. no. 225102.
[18] N. Liu, M. Mesch, T. Weiss, M. Hentschel, and H. Giessen, "Infrared perfect absorber and its application as plasmonic sensor," *Nano Lett.*, vol. 10, pp. 2342–2348, 2010.
[19] J. Hao, J. Wang, X. Liu, W. J. Padilla, L. Zhou, and M. Qiu, "High performance optical absorber based on a plasmonic metamaterial," *Appl. Phys. Lett.*, vol. 96, 2010, Art. no. 251104.
[20] J. Zhou, A. F. Kaplan, L. Chen, and L. J. Guo, "Experiment and theory of the broadband absorption by a tapered hyperbolic metamaterial array," *ACS Photon.*, vol. 1, pp. 618–624, 2014.
[21] Y. Cui *et al.*, "Ultrabroadband light absorption by a sawtooth anisotropic metamaterial slab," *Nano Lett.*, vol. 12, pp. 1443–1447, 2012.
[22] K. Aydin, V. E. Ferry, R. M. Briggs, and H. A. Atwater, "Broadband polarization-independent resonant light absorption using ultrathin plasmonic super absorbers," *Nature Commun.*, vol. 2, p. 517, 2011.
[23] V. Rinnerbauer *et al.*, "High-temperature stability and selective thermal emission of polycrystalline tantalum photonic crystals," *Opt. Exp.*, vol. 21, pp. 11482–11491, 2013.
[24] C. Argyropoulos, K. Q. Le, N. Mattiucci, G. D'Aguanno, and A. Alu, "Broadband absorbers and selective emitters based on plasmonic Brewster metasurfaces," *Phys. Rev. B.*, vol. 87, 2013, Art. no. 205112.
[25] E. S. Sakr, Z. Zhou, and P. Bermel, "High efficiency rare-earth emitter for thermophotovoltaic applications," *Appl. Phys. Lett.*, vol. 105, 2014, Art. no. 111107.
[26] J. Kischkat *et al.*, "Mid-infrared optical properties of thin films of aluminum oxide, titanium dioxide, silicon dioxide, aluminum nitride, and silicon nitride," *Appl. Opt.*, vol. 51, pp. 6789–6798, 2012.
[27] *RSoft CAD User Manual*, RSoft Design Group, Ossining, NY, USA, 2010, 8.2 ed.
[28] S. Preblea, M. Lipson, and H. Lipson, "Two-dimensional photonic crystals designed by evolutionary algorithms," *Appl. Phys. Lett.*, vol. 86, pp. 1–3, 2005.
[29] L. Shen, Z. Ye, and S. He, "Design of two-dimensional photonic crystals with large absolute band gaps using a genetic algorithm," *Phys. Rev. B*, vol. 68, pp. 1–5, 2003.
[30] A. Chipperfield, P. Fleming, H. Pohlheim, and C. Fonseca, *Genetic Algorithm Toolbox User Guide*. Sheffield, U.K.: Univ. Sheffield, 1994.
[31] H. Lipson and J. B. Pollack, "Automatic design and manufacture of robotic lifeforms," *Nature*, vol. 406, pp. 974–978, 2000.
[32] *MATLAB Global Optimization Toolbox User Guide*, MathWorks Inc., Natick, MA, USA, 2010.
[33] D. Chandler-Horowitz and P. M. Amirtharaj, "High-accuracy, midinfrared $(450\ \text{cm}^{-1} < \omega < 4000\ \text{cm}^{-1})$ refractive index values of silicon," *J. Appl. Phys.*, vol. 97, 2005, Art. no. 123526.
[34] F. Pratesi, M. Burresi, F. Riboli, K. Vynck, and D. S. Wiersma, "Disordered photonic structures for light harvesting in solar cells," *Opt. Exp.*, vol. 21, pp. A460–A468, 2013.
[35] E. R. Martins *et al.*, "Deterministic quasi-random nanostructures for photon control," *Nature Commun.*, vol. 4, p. 2665, 2013.
[36] C. Battaglia *et al.*, "Light trapping in solar cells: Can periodic beat random?" *ACS Nano*, vol. 6, pp. 2790–2797, 2012.
[37] A. Lin and J. D. Phillips, "Optimization of random diffraction gratings in thin-film solar cells using genetic algorithms," *Sol. Energy Mater. Sol.*, vol. 92, pp. 1689–1696, 2008.
[38] L. Yang, Y. Xuan, and J. Tan, "Efficient optical absorption in thin-film solar cells," *Opt. Exp.*, vol. 19, pp. A1165–A1174, 2011.